NASA Contractor Report 202346

# Laser-Induced Incandescence in Microgravity

Randall L. Vander Wal
*NYMA, Inc.*
*Brook Park, Ohio*

May 1997

Prepared for
Lewis Research Center
Under Contract NAS3–27186


National Aeronautics and
Space Administration

# LASER-INDUCED INCANDESCENCE IN MICROGRAVITY

RANDY L. VANDER WAL
NYMA @ NASA-Lewis
Cleveland, OH 44135

## Introduction

Knowledge of soot concentration is important due to its presence and impact upon a wide range of combustion processes ranging from diffusion to premixed flames, laminar to turbulent processes and homogeneous to heterogeneous combustion. Measurement of soot volume fraction ($f_v$) is essential to discerning its formation and growth [1]. The presence of soot also affects other physical and chemical properties of combustion thereby affecting studies not directly concerned with either its formation or growth, such as radiative heat transfer, CO oxidation and fuel vaporization or pyrolysis rates [1].

Microgravity offers unique opportunities for studying both soot growth and the effect of soot radiation upon flame structure and spread [2]. Spatial scales and residence time scales are greatly extended in 0-g facilitating soot growth studies. With the varied geometries, short duration microgravity test times and time-varying processes there is a demand for measurement of $f_v$ with high spatial and temporal resolution.

Laser-induced incandescence (LII) has advanced $f_v$ measurements in many 1-g combustion processes. To create laser-induced incandescence, a pulsed high intensity laser heats soot to incandescence temperatures [3]. Using appropriate spectral and temporal detection conditions, the resulting incandescence can be selectively detected apart from the non-laser-heated soot and flame gases. Theoretical modelling [4] and experiments [5-7] have shown that the resulting incandescence is representative of $f_v$. Using an intensified array camera and a laser sheet for excitation, one- and two-dimensionally resolved LII images of $f_v$ have been obtained in 1-g [6-10].

LII has been characterized and developed at NASA-Lewis for soot volume fraction determination in a wide range of 1-g combustion applications. Broadly grouped, the chacterization work has included studies of excitation intensity, excitation wavelength and the optimum temporal and spectral detection conditions to enable an accurate representation of soot volume fraction by LII [6,11]. Tests for special requirements imposed by different combustion processes have been performed in laminar [6,8,9] and turbulent [7,8] diffusion flames, rich sooting premixed flames [6], single droplet combustion [10], and other heterogeneous combustion. These studies demonstrated LII's high sensitivity, temporal and spatial capabilities and its geometric versatility.

In contrast to the advantages offered to combustion studies by a microgravity environment, advanced diagnostics, specifically those requiring pulsed laser diagnostics have been limited due to the size, weight and power limitations in a low-gravity environment. Reported here are the first demonstrations of LII performed in a microgravity environment. Examples are shown for laminar and turbulent gas-jet diffusion flames in 0-g.

## Experimental Approach

Experiments were performed in the 2.2 sec drop tower facility at NASA-Lewis [12].

To enable LII, light from a pulsed Nd:YAG laser is delivered via a 35 m long section of high OH-content, 1000 μm core diameter (30 μm cladding thickness) optical fiber to the drop package from the laser resident on the eigth floor of the drop tower. The jacket of the optical fiber consisted of black PVC with Kevlar-strengthening fibers. A special high power SMA-905 input connector was vital to coupling of the pulsed laser light into the optical fiber. Laser light at 532 nm from a short cavity, pulsed Nd:YAG laser manufactured by Big Sky Laser Inc. was coupled into the optical fiber using a 200 mm focal length plano-convex BK-7 lens. The combined input coupling efficiency of 532 nm light into the fiber plus transmission through the 35 m optical fiber was roughly 75%.

Figure 1 illustrates the layout of the drop rig. The divergence of the laser light at 532 nm emerging from the optical fiber is reduced by a 50-mm diameter, 100-mm-focal-length, fused-silica, spherical lens placed ~40 mm after the fiber. A laser sheet was formed using a 125 mm focal length 50 mm round cylindrical lens. Only the central 30 mm of the light sheet, representing the most uniform spatial intensity, was used for creating the laser-induced incandescence. A dichroic mirror following the cylindrical lens allowed for precise placement of the light sheet through the flame centerline. A beam dump

collected the laser light after the burner thereby eliminating scattered laser light. With an incident energy of 10 mj and estimated beam sheet width of 400 um, the laser intensity was roughly $1\times10^7$ W/cm$^2$.

LII images were detected by a ruggedized Xybion ISG-250 ICCD camera through a bandpass interference filter transmitting 400-450 nm. A glass lens used at f/8 fitted with a 10 mm extension tube provided a field-of-view (FOV) of about 30 mm. A custom electonics module provided power to the camera from the rig batteries and coupled the video and related timing signals out from the ICCD camera and gate pulse into the camera intensifier. Natural flame luminosity was detected by a Sony XC-77 black and white camera or a Sony XC-999 color video camera. Video signals from both cameras were transmitted though FM (6 MHz bandwidth) video transmitters attached to the drop rig, a dual fiber-optic video cable running between the drop rig and the top floor of the drop tower and FM video receivers located on the top floor of the drop tower. The LII signal was recorded on Beta video tape while the natural flame luminosity was recorded on SVHS video tape. A frame-grabber digitized images for subsequent analysis.

Synchronization of the laser, camera intensifier gate and camera video signal was achieved using custom electronics to detect the top-of-frame pulse on each LII video frame and provide a trigger pulse to a delay generator. The delay generator in turn triggered the laser and provided an inverted TTL pulse to serve as the gate pulse for the ICCD camera intensifier. The camera gate pulse was delivered through a 35 m length of BNC (RG58) cable connected to the camera control unit aboard the drop rig.

Drops were initiated by loading a computer program into an onboard droppable data acquisition/control system. This unit also controlled solid state relays to deliver power to the spark ignitor, cameras, and gas solenoid. A preburn prior to the drop ensured fuel within the gas-jet nozzle and confirmation of all systems working. Upon package release into free-fall, an electrical circuit was opened to provide a rising edge TTL trigger to initiate fuel delivery and ignition.

Laminar gas-jet diffusion flames were established on a 1.1 mm i.d. nozzle with approximately a 30° outside edge taper. The burner for the turbulent gas-jet diffusion flame utilized a 0.51 mm i.d. Nozzle (length/diameter >20) with a co-annular pilot diffusion flame. In each case a regulator and fine control valve were adjusted against a mass flow meter to deliver a known fuel flow rate. The acetylene flow through the central gas-jet tube was 1.0 slpm giving a Reynolds number of 4250 while the acetylene flow for the laminar coannular pilot flame was roughly 10 sccm.

## Results And Discussion

### *LII System Response*

Figure 2 illustrates the measured system dependence upon LII intensity. To test this dependence, a laminar steady-state gas-jet flame of ethylene was established in 1-g supported on the same 1.1 mm i.d. burner nozzle with a fuel flow rate of 48 sccm. The signal excitation and detection were configured as if the measurements were being performed in low-gravity. Consequently, the graph represents the results of an end-to-end test of the LII signal detection, transmitting and processing equipment which includes the intensified camera, the video fiber-optic transmitter plus receiver, beta recorder and the frame-grabber used for digitization of the video signal. With a fixed camera intensifier gain typical of that needed for LII 0-g measurements, the LII intensity reaching the camera was varied by placing calibrated neutral density filters in the optical path. Within the resulting digitized LII image, a region-of-interest (ROI) was defined containing 624 pixels within the flame tip where a rather spatially uniform $f_v$ distribution (<20% spatial intensity variation) was observed. The average pixel intensity within this region was calculated. Since the LII intensity incident upon the camera photocathode will vary as,

$$\text{Signal}_{(\text{det.})} = C * \text{LII} * 10^{(-\text{N.D.})}$$

where C is a constant, a semi-logarithmic plot of $\text{Signal}_{(\text{det.})}$ versus N.D. filter value should be linear provided all subsequent signal processing is linearly dependent upon the detected LII signal. This is observed in Fig. 2. The error bars represent one standard deviation of the ROI average intensity. Even if the curve were nonlinear, it would still provide a calibration curve for translating final digitized pixel intensities into relative LII intensities. The observed linearity allows straightforward interpretation of LII intensities as proportional to $f_v$.

### *Camera gain calibration*

Lower LII signals arising from lower soot concentrations could be readily detected by adjusting the camera intensifier gain. To establish the relative detection sensitivities at different intensifier gains, calibration measurements were performed. Again, the entire LII excitation/detection system was set up as if to perform low-gravity measurements. LII images of a laminar steady-state flame of ethylene (48 sccm flow rate) were acquired using different intensifier gains. Neutral density filters maintained the signal intensity within the dynamic range of the detection system. Analysis of a region of interest

(620 pixels) near the tip of the flame provided an average LII intensity for the particular gain setting (higher gains correspond to smaller readout values). Comparison of the relative LII intensities corrected for the neutral density filter attenuation provided a relative measure of the detection sensitivity at the different gain settings. To faciliate comparison, the relative values were normalized by the LII average intensity measured with the lowest practical gain setting. These results are shown in Fig. 3. The error bars were calculated assuming Poisson statistics with the standard deviation calculated as the square root of the average LII pixel intensity. These limits were found empirically to well encompass the variation observed in the average LII intensity calculated within the ROI.

Although the semi-logarithmic plot conveniently illustrates the range of detection sensitivities, there is a physical basis for this method of plotting. Because the photon detection event is described by a Poisson distribution [13] and the intensifier amplification process is exponential [14], with a linear detection system, the detected signal intensity would be expected to scale exponentially with the intensifier gain provided no saturation of the electron multiplication process occured within the microchannel plate, coupled phosphor screen or CCD pixel well. As Fig. 3 shows, using the intensifier, more than a 1000-fold increase in detection sensitivity can be achieved relative to that at a gain setting of 4.70. Based on soot volume fractions of about 15 ppm for the laminar 50/50 (v/v) acetylene/nitrogen mixture in 1-g detected using a gain of 4.70, a detection sensitivity of nearly 0.01 ppm is predicted based on Fig. 3

*Validation of LII*

Figure 4 shows LII images of a laminar acetylene gas-jet diffusion flame in 1-g and 0-g with a fuel flow rate of 70 sccm. The effect of buoyancy upon the flame shape and soot processes is clear. Buoyancy induced air entrainment causes radial confinement of the gas-jet in 1-g. In 0-g, the initial fuel-jet momentum governs the flow with the divergence of the gas-jet clearly observed from the soot spatial distribution. In contrast to 1-g, flow trajectories in 0-g follow a monotonic path in mixture fraction and temperature while within the flame leading to extended spatial scales for soot inception and subsequent growth.

To verify the validity of the LII measurements as representative of $f_v$, LII radial intensity profiles from the acetylene gas-jet flame in 0-g are compared with those derived from a full-field extinction method that has been reported previously [15]. The axial positions were chosen to illustrate different spatial and intensity variations in $f_v$. Three radial pixel rows of the LII image were averaged together for better signal-to-noise thus giving a spatial resolution of 0.25 mm. Each LII profile was also corrected for attenuation by soot between the LII image plane and camera. To convert the relative LII intensities to $f_v$, each LII radial profile was multiplied by a scaling factor which was determined by the ratio of the summed LII intensity from all radial profiles to the radially summed $f_v$'s at the same axial positions. As can be seen from Fig. 5, good agreement is observed between the LII measurements and those derived from extinction where both the relative spatial variations and intensities are similar. While previous tests of LII have shown it to yield accurate relative measurements in 1-g by comparison with light extinction and gravimetric sampling, these results are the first tests validating LII as a diagnostic for $f_v$ in 0-g.

Additional Demonstrations

*Laminar gas-jet flame*

Figure 6 shows LII images obtained from a laminar ethane gas-jet diffusion flame in 1-g and 0-g. In each case, the fuel flow rate was 70 sccm with resulting Reynolds number of 200. Due to buoyancy-induced instabilities, the normal gravity flame frequently flickered, consequently a representative image was chosen. As clearly seen by Fig. 6, buoyant acclceration overcomes the divergent cold-gas flow causing radial confinement of the flame in 1-g. With soot oxidation proceeding inward towards the flame centerline, soot on the jet centerline is oxidized last resulting in the steeple shaped soot distribution at the flame tip. With buoyant acceleration eliminated in 0-g, the initial divergence of the exiting fuel flow is largely preserved resulting in a flame spatial extent determined much more by stoichiometry requirements than in 1-g. Similar to the laminar gas-jet flame of acetylene, absence of buoyant entrainment leads to an increase in the spatial extent of soot inception and growth. Despite the fuel abundance within the central core of the flame, a combination of insufficient fuel pyrolysis products and diminished temperatures relative to 1-g likely inhibit soot formation reactions along the axial streamline resulting in the absence of soot at the flame tip.

Although the flicker observed in 1-g causes variation in peak $f_v$ (ranging from 0.3 to 0.6 ppm in the tip of the flame), the ratio of the 0-g to 1-g $f_v$ is roughly 3 based on a comparison of LII intensities. This example also illustrates the sensitivity of LII as the radially integrated $f_v$-pathlength product is $6.7\times10^{-7}$ cm yielding a transmittance of 0.95 using Ke = 4.9 from Dazell and Sarofim [16]. Such a high transmittance is marginally detectable using unstabilized HeNe lasers, voltage biased photodetectors and 8-bit digitization. On the basis of the camera gain calibration curve, approximately a factor of 30 higher sensitivity (or a factor of 30 lower $f_v$) is achievable using a camera gain of 4.40 compared to 4.575 as was presently

used. Such a high transmittance is likely undetectable even using sensitive lock-in detection of absorbance which possesses a practical limit of roughly 0.1 % absorbance sensitivity with RC timeconstants on the order of 100s' of msec.

*Turbulent gas-jet flame*

Figure 7a, perhaps the best illustration of the temporal plus spatial capabilities of LII and its geometric versatility, shows a LII image from a turbulent gas-jet flame of acetylene with Reynolds number of 4250 in 0-g. Even using a detection gate of 500 ns to ensure capture of the of the LII signal, temporal frequencies of greater than 1 MHz can be frozen. As determined using a replica of the 1951 Air Force test pattern, the spatial resolution is approximately 5 line pairs per millimeter allowing spatial structures of 0.1 mm to be resolved. Figure 7b is a contour plot of Fig. 7a. Absolute soot volume fractions were calculated based on the LII image intensity in the turbulent flame relative to that of the reference flame system using the camera intensifier calibration curve of Fig. 3.

*Vortex visualization*

Figure 8 is a LII image of soot within a vortex formed by propane fuel issuing from a gas-jet nozzle. The central bulge is due to the initial jet momentum while the side recirculation regions result from air entrainment into the shear layer. Initiation of fuel flow and subsequent ignition were performed in low-gravity (after package release from the "music" wire). The nominal jet Reynold's number was 330 based on the nozzle ID of 1.1 mm and flow rate of 70 sccm. The higher $f_v$ in the recirculation regions is sensible as fuel parcels in these regions experience extended times at elevated temperatures promoting fuel pyrolysis processes and soot growth. The transient vortex and steep spatial gradients require the temporal and spatial capabilities of LII.

## Conclusions

Combustion processes exhibit rather different features in microgravity compared to normal gravity. With the elimination of buoyancy-induced convection, both flame shape and $f_v$ differ substantially compared to the same fuel/burner system in normal gravity. The sensitivity, temporal and spatial capabilities in addition to geometric versatility enable LII to reveal the soot volume fraction regardless of these differences. Comparison of radial $f_v$s obtained by light extinction and LII validate LII for $f_v$ determination in low-gravity. Application of LII to a laminar gas-jet flame of ethane illustrates the sensitivity of LII while application to a turbulent diffusion flame of acetylene and vortex formed by a transient gas-jet diffusion flame of propane demonstrate the high temporal and spatial capabilities of LII for $f_v$ determination. Spatial and concentration differences of $f_v$ in 1-g and 0-g environments are readily illustrated by comparison of the LII images.

## Acknowledgements

This work was supported through NASA contract, NAS3-27186. The author thanks Prof. J.C. Ku (Wayne State University) and P.S. Greenberg (NASA-Lewis) for sharing their full-field light extinction data.

## Disclaimer

Manufacturer and product names are used to aid understanding and do not constitute an endorsement by the federal government.

## References

1. Soot Formation in Combustion, (H. Bockhorn Ed.), Springer-Verlag, Heidelberg, (1994).
2. Proceedings of the Third International Microgravity Combustion Workshop, (NASA CP-10174), April 11-13, Cleveland, OH (1995).
3. Eckbreth, A.C., Laser Diagnostics for Combustion Temperature and Species, Gordon and Breach, Amsterdam, The Netherlands, 2nd ed. 1996. p. 254.
4. Melton, L.A., Appl. Opt. 23:2201 (1984).
5. Quay, B., Lee, T.W., Ni, T. and Santoro, R.J., Combust. and Flame 97:394 (1994).
6. Vander Wal, R.L. and Weiland, K.J., J. Appl. Phys. B59:445 (1994).
7. Vander Wal, R.L., Zhou, Z. and Choi, M.Y., Combust. And Flame 105:462 (1996).
8. Ni, T., Pinson, J.A., Gupta, S. and Santoro, R.J., Appl. Opt. 34:7083 (1995).
9. Shaddix, C.R. and Smyth, K.C. Combust. And Flame 107:418-452 (1996).
10. Vander Wal, R.L. and Dietrich, D.L. Appl. Opt. 34:1103 (1995).
11. Vander Wal, R.L., Appl. Opt. 35:6548 (1996).
12. Lekan, J., Gotti, D.J., Jenkins, A.J., Owens, J.C. and Johnston, M.R., NASA TM-107090, April, (1996).
13. Stanford Research Systems, Application Notes, 1996-1997, Note no. 4, p. 186.
14. Engstrom, R.W., RCA Photomultplier handbook, The RCA Corporation, (1980).
15. Greenberg, P.S. and Ku, J.C. Combust. And Flame 108:227-230 (1997).
16. Dalzell, W.H. and Sarofim, A.L. J. Heat Transfer 91:100-106 (1969).

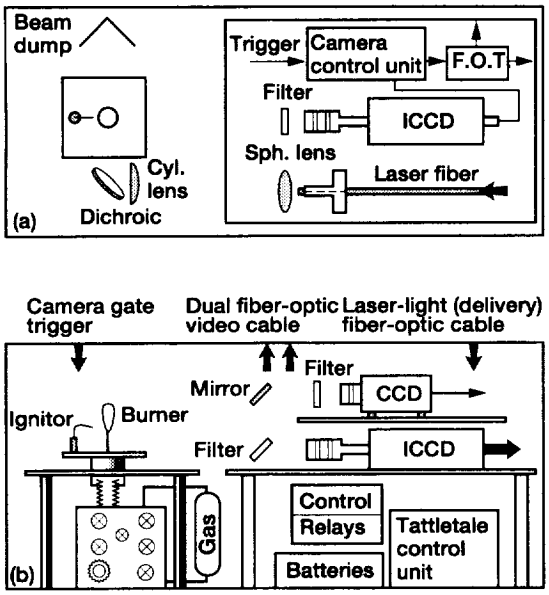


Figure 1.—(a) Top view of the hardware and optical layout of the drop rig. (b) Corresponding side view.

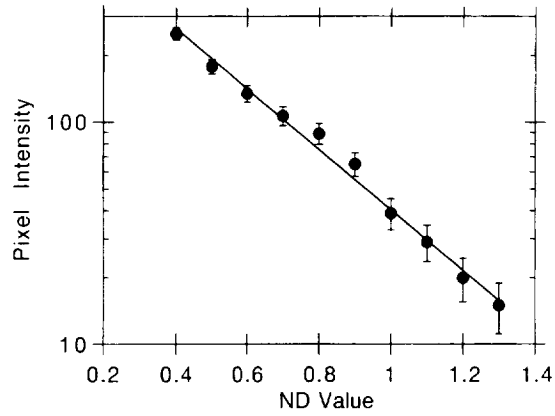


Figure 2.—Average LII pixel intensity versus neutral density filter value (ND) preceding the LII camera. See text for details.

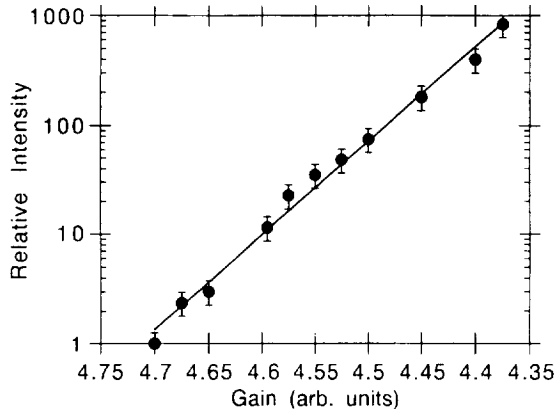


Figure 3.—Camera intensifier gain calibration curve. Note that higher intensifier gains correspond to smaller values of the gain setting. See text for details.

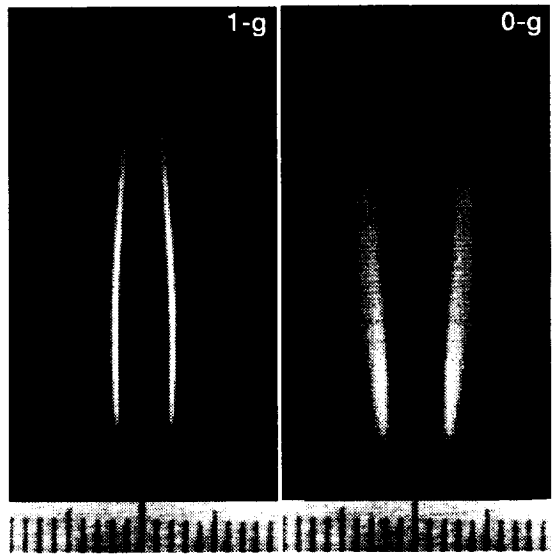


Figure 4.—LII images of a laminar acetylene gas-jet diffusion flame in 1-g and 0-g. The burner nozzle is 1 mm above the picture bottom (but is not observable in the LII images). The ruler spatial scale is in millimeters.

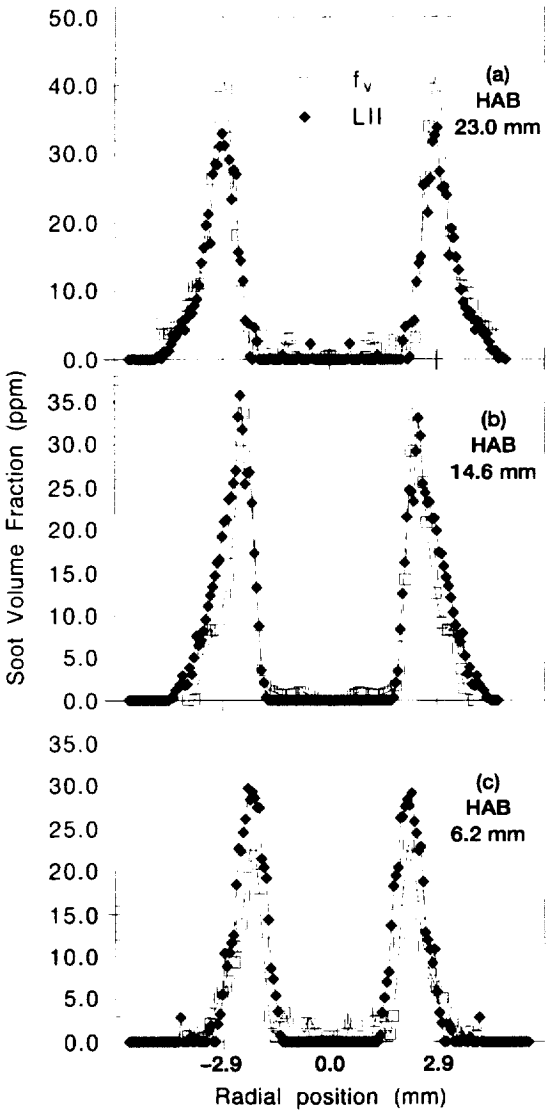


Figure 5.—Comparison of LII radial intensities with $f_v$ determined through light extinction in the laminar gas-jet flame of acetylene in 0-g (shown in Fig. 4) at the indicated axial heights above the burner.

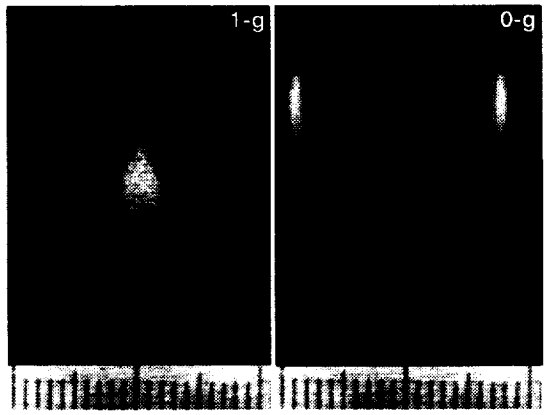


Figure 6.—LII images of a laminar ethane gas-jet diffusion flame in 1-g and 0-g. The burner nozzle is 11 mm below the picture bottom. The ruler spatial scale is in millimeters. See text for details.

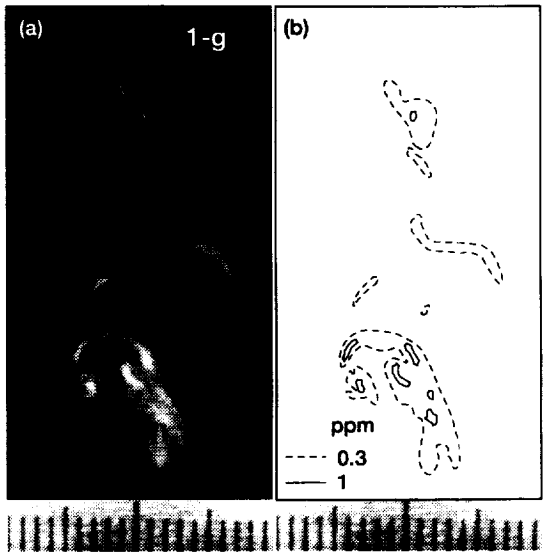


Figure 7.—(a) LII image of soot within the oxidation region of a turbulent gas-jet flame of acetylene. (b) Contour plot of (a) with $f_v$ values given in ppm. The image bottom is 100 mm above the burner nozzle. The ruler spatial scale is in millimeters.

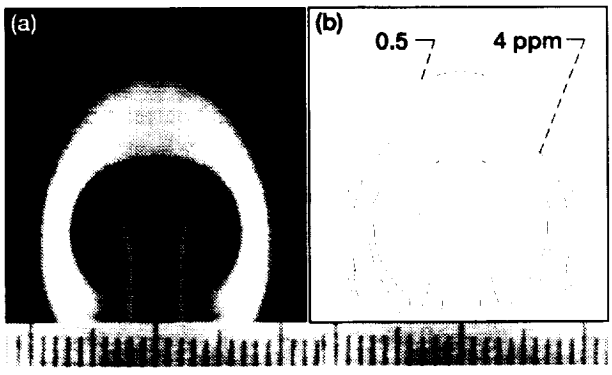


Figure 8.—(a) LII image of a vortex formed during initial formation of a laminar gas-jet flame of propane in 0-g. (b) Contour plot of (a) with $f_v$ values given in ppm. Both fuel flow and ignition were initiated in 0-g. The nominal steady-state fuel flow rate was 70 sccm. The burner nozzle is 11 mm below the picture bottom. See text for details.

# REPORT DOCUMENTATION PAGE

Form Approved
OMB No. 0704-0188



| 1. AGENCY USE ONLY (*Leave blank*) | 2. REPORT DATE | 3. REPORT TYPE AND DATES COVERED |
|---|---|---|
| | May 1997 | Final Contractor Report |

**4. TITLE AND SUBTITLE**

Laser-Induced Incandescence in Microgravity

**5. FUNDING NUMBERS**

WU–963–70–0E
C–NAS3–27186

**6. AUTHOR(S)**

Randall L. Vander Wal

**7. PERFORMING ORGANIZATION NAME(S) AND ADDRESS(ES)**

NYMA, Inc.
2001 Aerospace Parkway
Brook Park, Ohio 44142

**8. PERFORMING ORGANIZATION REPORT NUMBER**

E–10682

**9. SPONSORING/MONITORING AGENCY NAME(S) AND ADDRESS(ES)**

National Aeronautics and Space Administration
Lewis Research Center
Cleveland, Ohio 44135–3191

**10. SPONSORING/MONITORING AGENCY REPORT NUMBER**

NASA CR–202346

**11. SUPPLEMENTARY NOTES**

Prepared for the International Microgravity Combustion Workshop sponsored by NASA Lewis Research Center, May 19–21, 1997. Project Manager, Howard D. Ross, Space Experiments Division, NASA Lewis Research Center, organization code 6711, (216) 433–2562.

**12a. DISTRIBUTION/AVAILABILITY STATEMENT**

Unclassified - Unlimited
Subject Category 25

This publication is available from the NASA Center for AeroSpace Information, (301) 621–0390.

**12b. DISTRIBUTION CODE**

**13. ABSTRACT** ***(Maximum 200 words)***

Microgravity offers unique opportunities for studying both soot growth and the effect of soot radiation upon flame structure and spread. LII has been characterized and developed at NASA-Lewis for soot volume fraction determination in a wide range of 1-g combustion applications. Reported here are the first demonstrations of LII performed in a microgravity environment. Examples are shown for laminar and turbulent gas-jet diffusion flames in 0-g.

**14. SUBJECT TERMS**

Soot; LII; Laser-induced incandescence; Microgravity

**15. NUMBER OF PAGES**

8

**16. PRICE CODE**

A02

| 17. SECURITY CLASSIFICATION OF REPORT | 18. SECURITY CLASSIFICATION OF THIS PAGE | 19. SECURITY CLASSIFICATION OF ABSTRACT | 20. LIMITATION OF ABSTRACT |
|---|---|---|---|
| Unclassified | Unclassified | Unclassified | |